ISSN 0020-1685, Inorganic Materials, 2006, Vol. 42, No. 12, pp. 1326–1335. © Pleiades Publishing, Inc., 2006.
Original Russian Text © V.A. Somenkov, S.A. Lushnikov, V.P. Glazkov, V.N. Verbetsky, 2006, published in Neorganicheskie Materialy, 2006, Vol. 42, No. 12, pp. 1454–1463.

Structure and Bonding Configuration of Hydrided $ErNi_3$ and $CeCo_3$

V. A. Somenkov[a], S. A. Lushnikov[b], V. P. Glazkov[a], and V. N. Verbetsky[b]

[a] *Russian Research Centre Kurchatov Institute, pl. Kurchatova 1, Moscow, 123182 Russia*
[b] *Moscow State University, Vorob'evy gory 1, Moscow, 119992 Russia*
e-mail: lushnikov@hydride.chem.msu.ru

Received February 20, 2006

Abstract—The intermetallic compounds $ErNi_3$ and $CeCo_3$ has been hydrided at low ($p_{H_2} \le 0.01$ GPa) and high (p_{H_2} up to 0.2 GPa) hydrogen pressures. X-ray and neutron diffraction characterization has shown that the resultant hydrides have structures of the same type ($PuNi_3$) as the parent intermetallics and have a larger unit-cell volume. We have identified the positions occupied by the metal and hydrogen atoms and have determined their positional parameters. The lattice anisotropy has been shown to vary little at high hydrogen concentrations. Our results indicate that the metal–hydrogen bonds in the hydrides studied are predominantly ionic for the rare-earth metals (Er and Ce) and predominantly metallic for the transition metals (Ni and Co).

DOI: 10.1134/S0020168506120089

INTRODUCTION

In studies of the interaction between intermetallic compounds and hydrogen, particular interest has been centered on RT_3 (R = rare-earth metal, T = transition metal) compounds having $PuNi_3$-type structures. The reason is that these compounds are commonly thought of as consisting of blocks of well-known compounds with the RT_2 ($MgZn_2$ structure) and RT_5 ($CaCu_5$ structure) stoichiometries, stacked along the *c* axis, and are intermediate in structure between these two types of compounds. Given that the hydrogen affinity of the rare-earth metals is higher than that of the transition metals and that the blocks differ in R : T ratio, it is reasonable to expect a marked preference of hydrogen atoms between the two types of blocks: hydrogen must be accommodated first in the RT_2 blocks and then in the RT_5.

Structural studies revealed significant differences in hydrogen accommodation and associated lattice distortions between low-pressure hydrides with such structures [1–4]. The hydriding of some compounds (R = Ce, La, Pr, Nd) was found to give rise to a significant anisotropic lattice expansion, whereas other hydrides (R = Ho, Er) show insignificant lattice anisotropy. This behavior of intermetallic hydrides can be rationalized in terms of the nature of hydrogen accommodation or the interaction between hydrogen and metal atoms. Recent work by Latroche et al. [5] has shown that, in the compounds CeY_2Ni_9 and LaY_2Ni_9, similar in structure to the $PuNi_3$ type, the hydrogen-induced lattice expansion is isotropic if the hydrogen is accommodated in both the RT_2 and RT_5 blocks (LaY_2Ni_9) and anisotropic if only the RT_2 blocks absorb hydrogen (CeY_2Ni_9). At high pressures and, accordingly, increased hydrogen concentrations in intermetallic hosts, one would expect hydrogen accommodation in both types of blocks and, hence, changes in lattice anisotropy. It is, therefore, of interest to find out in which sequence different types of blocks and sites are occupied by hydrogen and to evaluate the anisotropy of high-pressure hydrides.

In this paper, we report a structural study of $ErNi_3$ and $CeCo_3$ hydrided at high hydrogen pressures. At low hydrogen concentrations, these intermetallics differ in lattice anisotropy.

EXPERIMENTAL

The $ErNi_3$ and $CeCo_3$ alloys were prepared by arc-melting pure metals in an inert atmosphere and were then annealed at 1220 K for 240 h in an evacuated silica tube. Deuterides were synthesized in a high-pressure apparatus (p_{D_2} up to 0.2 GPa [6]) and Sieverts apparatus ($p_{D_2} \le 0.01$ GPa) using high-purity hydrogen generated by the $LaNi_5$ and TiFe hydrogen-storage alloys. To avoid the formation of x-ray amorphous materials, deuterium was introduced into the reactor in portions at a pressure $p_{D_2} \le 1$ MPa, and after each portion the reaction was given time to reach completion. To prevent deuterium release from the deuterides, they were cooled to liquid-nitrogen temperature immediately after synthesis, and then low-temperature neutron diffraction studies were performed. The amount of absorbed deuterium was determined by thermal desorp-

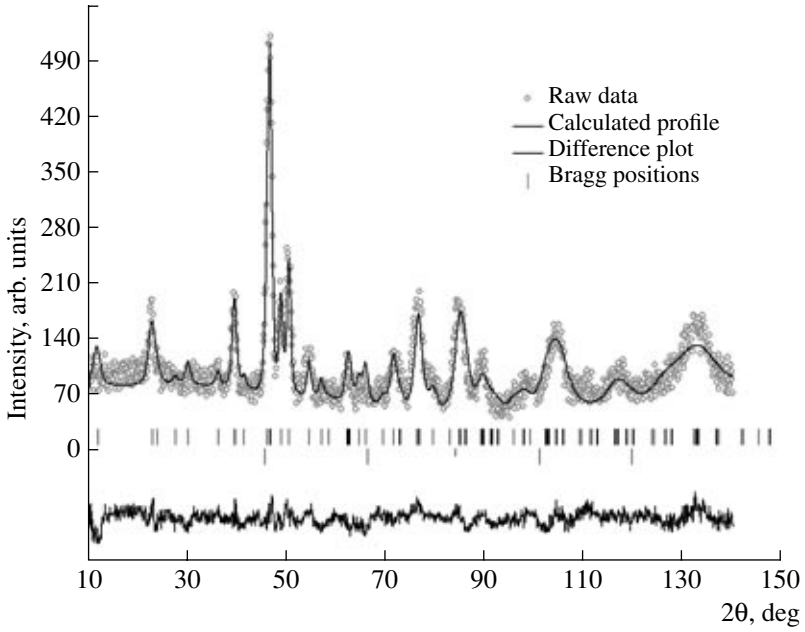

Fig. 1. Neutron diffraction pattern of $ErNi_3$.

tion measurements. X-ray diffraction (XRD) patterns were collected on Rigaku and ThermoARL diffractometers. Neutron diffraction measurements were performed on a DISK diffractometer at the Russian Research Centre Kurchatov Institute. The data were analyzed by the Rietveld method using Fullprof software. To reduce incoherent neutron scattering, we used deuterium instead of hydrogen.

RESULTS AND DISCUSSION

We studied the $ErNi_3D_{4.0}$ and $CeCo_3D_{4.0}$ hydrides synthesized at low hydrogen pressure, and $ErNi_3D_{5.0}$ and $CeCo_3D_{6.0}$ synthesized at high pressure. According to XRD and neutron diffraction results, the $ErNi_3$ (Fig. 1) and $CeCo_3$ alloys were single-phase, and their lattice parameters agreed with earlier data [7]. The hydrides had the same structure ($PuNi_3$ type) as the parent intermetallics. $ErNi_3D_{4.0}$ was synthesized at low temperature since, according to earlier results [8], the $ErNi_3$–H_2 system at low hydrogen pressures contains two hydrides differing in hydrogen content.

Both XRD and neutron diffraction data indicate that the unit-cell volume of the hydrides is a nonlinear function of hydrogen content. The volume per hydrogen atom decreases with increasing hydrogen content (Table 1), so that the hydrogen-induced volume effect in the completely hydrided materials ($ErNi_3D_{5.0}$ and $CeCo_3D_{6.0}$) is smaller than that in the partially hydrided ones ($ErNi_3D_{4.0}$ and $CeCo_3D_{4.0}$). This behavior is characteristic of rare-earth hydrides and hydrided rare-earth-rich RT_2 intermetallics ($GdFe_2H_x$, $HoFe_2H_x$), whereas the unit-cell volume of transition-metal hydrides and hydrided transition-metal compounds is a linear function of hydrogen content. As shown earlier [9], these features of the hydrogen-induced volume effect are related to the fact that hydrogen forms different bonds with transition metals and rare earths, acting as an acceptor in R–H bonds and as a donor in T–H bonds, which corresponds to emptying of the *sp* band in the rare-earth hydrides and filling of the *d* band in the transition-metal hydrides. Structural data (Table 1, Fig. 2) indicate that hydrogen-poor hydrides differ in the increase in unit-cell volume per hydrogen atom and *c*/*a* ratio: these parameters are smaller in $ErNi_3D_{4.0}$ (heavy rare-earth metal) and larger in $CeCo_3D_{4.0}$ (light rare-earth metal). Similar relationships were reported earlier for other hydrided RNi_3 intermetallics with the same structure and nearly the same hydrogen content [10–12] (Table 2). According to XRD data, the *c*-axis positional parameters of the metal atoms (Table 1, Fig. 2) are highly sensitive to hydrogen content in the case of large anisotropy ($CeCo_3D_{4.0}$) and vary little in the case of small anisotropy ($ErNi_3D_{4.0}$). Thus, the hydrides containing light (Ce) and heavy (Er) rare-earth metals differ in the hydrogen-induced volume effect, anisotropy, and positional parameters of metal atoms. It is, therefore, of interest to find out in what measure these distinctions are associated with the nature of the sites occupied by hydrogen in the intermetallics.

The exact nature of hydrogen sites in intermetallic hosts such as RT_3 is rather difficult to assess from neutron diffraction data by the Rietveld method because acceptable agreement between experimental data and calculation results can be achieved in different ways, depending on the number of refinement parameters and relations between them. In view of this, we attempted

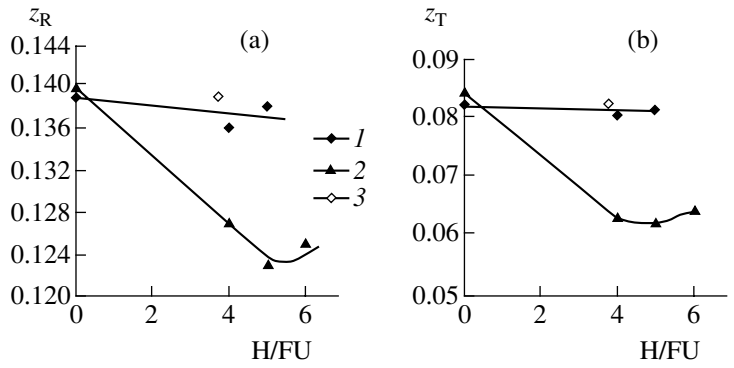

Fig. 2. Positional parameters of metal atoms as functions of hydrogen content (hydrogen atoms per formula unit) for hydrided (*1*, *3*) $ErNi_3$ (this work and [2], respectively) and (*2*) $CeCo_3$.

not only to identify the sites occupied by hydrogen and to contrast the results with data for low-pressure hydrides but also to compare different structural models in order to assess their credibility. To reduce the number of refinement parameters, we used the positional parameters of metal atoms determined by XRD at different hydrogen contents and fixed the Debye–Waller factors of the rare earth, transition metal, and

Table 1. Hydrogen-induced volume effect and structural parameters in hydrided $ErNi_3$ and $CeCo_3$

Composition	*a*, nm	*c*, nm	$V \times 10^3$, nm^3	$\Delta V/V$, %	$\Delta V/H \times 10^3$, nm^3*	z_R	z_T
$ErNi_3$ [8]	0.4944(1)	2.425(2)	513	–	–	–	–
$ErNi_3$	0.4943(2)	2.428(2)	514	–	–	0.139(2)	0.082(1)
$ErNi_3D_{1.23}$ [2]	0.4972(2)	2.590(1)	554	7.6	3.5	0.131(2)	0.073(2)
$ErNi_3D_{1.97}$ [2]	0.5240(3)	2.561(2)	577	12.0	3.5	0.131(3)	0.078(2)
$ErNi_3D_{3.8}$ [2]	0.5240(3)	2.561(2)	633	23.2	3.5	0.139(1)	0.082(3)
$ErNi_3D_{4.0}$	0.5271(2)	2.665(2)	641	25.2	3.6	0.136(2)	0.080(3)
$ErNi_3D_{5.0}$	0.5294(3)	2.670(1)	648	26.6	3.0(0.8)**	0.138(1)	0.081(2)
$CeCo_3$ [8]	0.4994(2)	2.461(1)	532	–	–	–	–
$CeCo_3$	0.4961(1)	2.480(3)	529	–	–	0.140(2)	0.084(1)
$CeCo_3D_{4.0}$	0.4936(3)	3.245(2)	684	29.3	4.3	0.127(3)	0.063(3)
$CeCo_3D_{5.0}$	0.4580(2)	3.254(3)	694	31.2	3.7(1.0)**	0.123(3)	0.062(2)
$CeCo_3D_{6.0}$	0.4980(1)	3.265(2)	701	32.5	3.2(0.9)**	0.125(2)	0.064(4)

* Increase in unit-cell volume per adsorbed hydrogen atom.

** Increase in unit-cell volume per adsorbed hydrogen atom in going from low- to high-pressure hydrides.

Table 2. Hydrogen-induced volume effect in RNi_3H_4

R	*a*, Å	*c*, Å	*c*/*a*	*V*, Å^3	$\Delta V/V$, %	ΔV/H, Å^3*
La [10]	5.011	33.12	6.095	720	28.3	4.4
Pr [10]	4.959	32.90	6.606	701	25.8	4.0
Nd [10]	4.957	32.20	6.496	685	25.9	3.9
Sm [11]	5.320	27.06	5.086	663	23.8	3.5
Tb [12]	5.302	26.78	5.051	651	24.0	3.3

* Increase in unit-cell volume per adsorbed hydrogen atom.

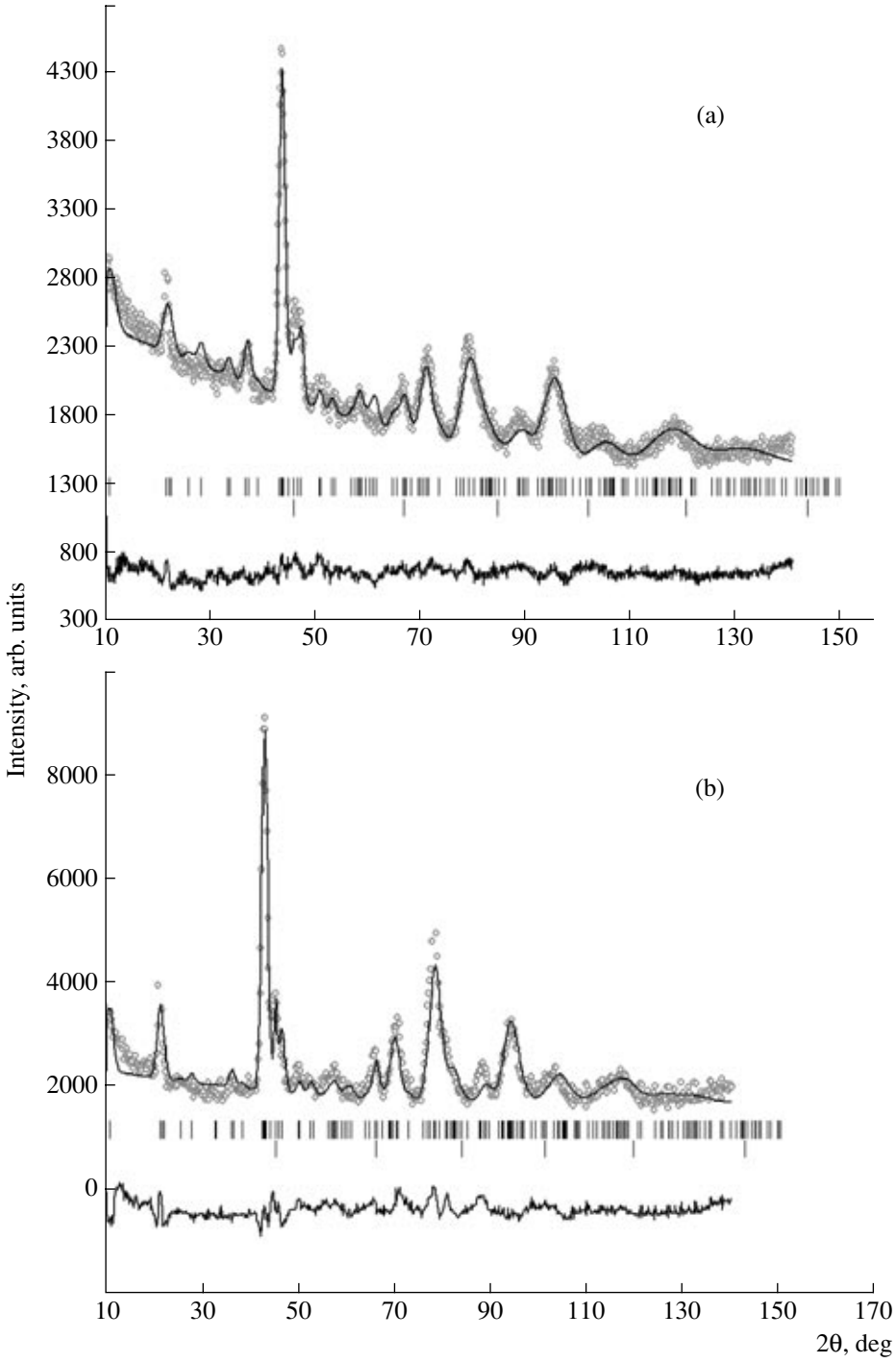

Fig. 3. Neutron diffraction patterns of (a) $ErNi_3D_{4.0}$ and (b) $ErNi_3D_{5.0}$; same designations as in Fig. 1.

deuterium ($2B$ = 0.8, 0.4, and 2.0, respectively). Next, using neutron diffraction data (Fig. 3), we determined the positions and positional parameters of the deuterium atoms.

Our calculations indicate that, in the $CeCo_3D_{4.0}$ and $ErNi_3D_{4.0}$ hydrides (Table 3, Figs. 4, 5), hydrogen resides predominantly in position $36i_1$ of the RT_2 block. Similar hydrogen distributions were reported by Filinchuk and Yvon [2] for the $ErNi_3D_x$ (x = 1.23, 1.97, 3.75) hydrides. Their results demonstrate that, at the lowest hydrogen content ($ErNi_3D_{1.23}$), hydrogen is accommodated in the RT_2 block, while increasing the hydrogen content ($ErNi_3D_{1.97}$) causes hydrogen to occupy, in addition, sites common to the RT_2 and RT_5 blocks and also sites in the RT_5 block. In the $ErNi_3D_{3.75}$ hydride, which is the closest in synthesis conditions (low tem-

Table 3. Crystal data for $ErNi_3D_{4.0}$, $ErNi_3D_{5.0}$, $CeCo_3D_{4.0}$, and $CeCo_3D_{6.0}$

Atom	Position	Atoms per unit cell	x	y	z	Atoms per unit cell	x	y	z
		$ErNi_3D_{4.0}$				$ErNi_3D_{5.0}$			
Er(1)	3*a*	3.0	0	0	0	3.0	0	0	0
Er(2)	6*c*	6.0	0	0	0.136(2)	6.0	0	0	0.138(1)
Ni(1)	3*b*	3.0	0	0	0.5	3.0	0	0	0.5
Ni(2)	6*c*	6.0	0	0	0.321(2)	6.0	0	0	0.327(2)
Ni(3)	18*h*	18.0	0.493(1)	−0.493(1)	0.080(3)	18.0	0.503(1)	−0.503(1)	0.081(3)
D(1)	$36i_2$	3.6(2)	0.445(3)	0.010(2)	0.003(2)	4.30(3)	0.450(2)	0.006(2)	0.008(2)
D(2)	$18h_3$	7.2(2)	0.760(2)	−0.760(3)	0.124(3)	7.60(2)	0.758(2)	−0.758(2)	0.129(2)
D(3)	$36i_1$	25.3(2)	0.472(3)	0.008(2)	0.135(3)	28.8(2)	0.469(2)	0.012(2)	0.140(2)
D(4)	$9e_1$	–	–	–	–	5.4(1)	0.5	0.5	0
		R_p = 12.0%, R_w = 8.8%, R_B = 14.6%, D/FU = 4.0				R_p = 11.0%, R_w = 8.0%, R_B = 12.2%, D/FU = 5.1			
		$CeCo_3D_{4.0}$				$CeCo_3D_{6.0}$			
Ce(1)	3*a*	3.0	0	0	0	3.0	0	0	0
Ce(2)	6*c*	6.0	0	0	0.127(2)	6.0	0	0	0.125(1)
Co(1)	3*b*	3.0	0	0	0.5	3.0	0	0	0.5
Co(2)	6*c*	6.0	0	0	0.321(2)	6.0	0	0	0.327(2)
Co(3)	18*h*	18.0	0.502(1)	−0.502(1)	0.063(3)	18.0	0.504(1)	−0.504(1)	0.064(4)
D(1)	$18h_2$	8.50(3)	0.850(2)	−0.850(2)	0.068(3)	10.80(3)	0.843(2)	−0.843(2)	0.070(2)
D(2)	$36i_1$	27.80(3)	0.461(2)	0.009(4)	0.127(3)	21.20(2)	0.462(3)	0.010(1)	0.129(3)
D(3)	$36i_2$	–	–	–	–	14.80(2)	0.450(2)	0.012(3)	−0.003(2)
D(4)	$9e_1$	–	–	–	–	5.90(2)	0.5	0.5	0.0
		R_p = 9.2%, R_w = 9.0%, R_B = 15.1%, D/FU = 4.0				R_p = 11.6%, R_w = 10.7%, R_B = 12.4%, D/FU = 5.9			

perature) and composition to $ErNi_3D_{4.0}$, hydrogen resides predominantly in the RT_2 block, while positions in the RT_5 block and between the blocks have lower occupancies. The slight differences in site occupancies can be accounted for by different experimental conditions: $ErNi_3D_{3.75}$ was studied at room temperature [2], while $ErNi_3D_{4.0}$, at liquid-nitrogen temperature (77 K). In this study, the calculated profiles do not fit the experimental data very well. Calculations indicate that the agreement can be improved by introducing additional fitting parameters (low-occupancy sites which make only a small contribution to the scattering power), varying the Debye–Waller factor, etc. It is not, however, clear whether such changes are meaningful because of the large number of fitting parameters and relatively small number of well-resolved peaks. Moreover, comparison of different models for RT_3D_4 hydrides [2, 4, 5] shows that they differ little (relative difference in R factor is less than 5%). Our neutron diffraction data indicate that, in the structures of $ErNi_3D_{4.0}$ and $CeCo_3D_{4.0}$, which differ in anisotropy (c/a) and hydrogen-induced volume effect, most of the hydrogen atoms reside in the same position ($36i_1$) of the RT_2 block, so that the structural distinctions between these hydrides and their anisotropy are not directly related to the hydrogen distribution. The hydrogen content determined by thermal desorption measurements differs insignificantly from that inferred from neutron diffraction data.

In the structure of other hydrided RT_3 compounds with a low hydrogen concentration, hydrogen also resides predominantly in positions i and h of the RT_2 block (Table 4) [1, 2, 4, 5]. In addition, hydrogen occupies sites with R_2M_2 coordination, shared by RT_2 and RT_5 blocks, but the occupancy of such sites is, as a rule, lower.

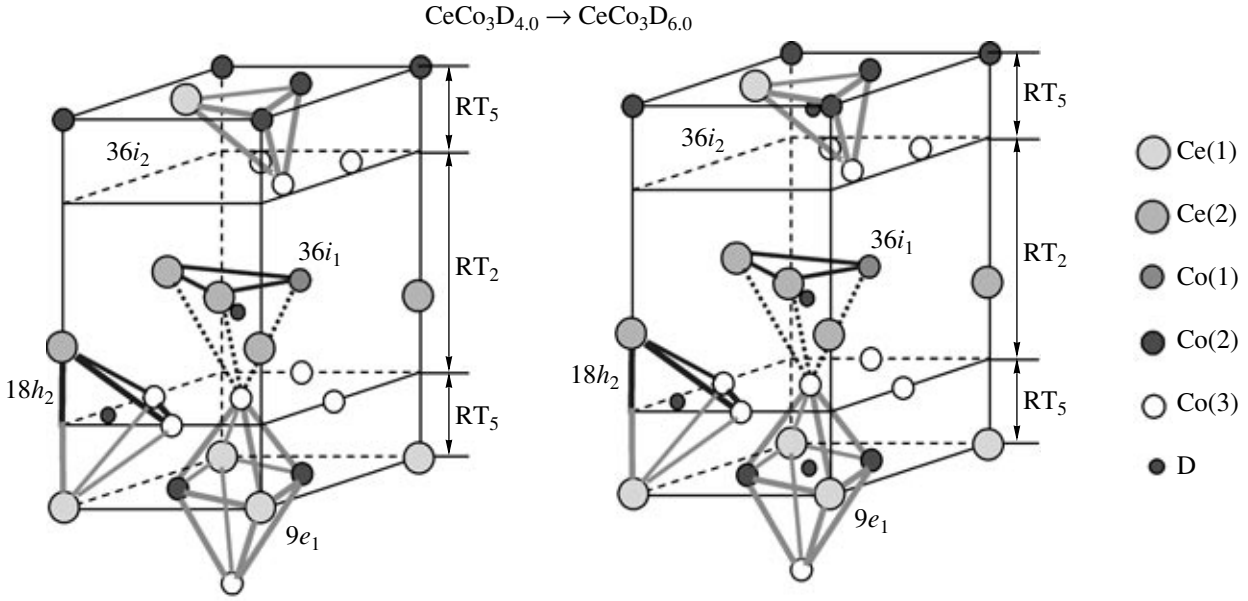

Fig. 4. Hydrogen sites in hydrided $CeCo_3$.

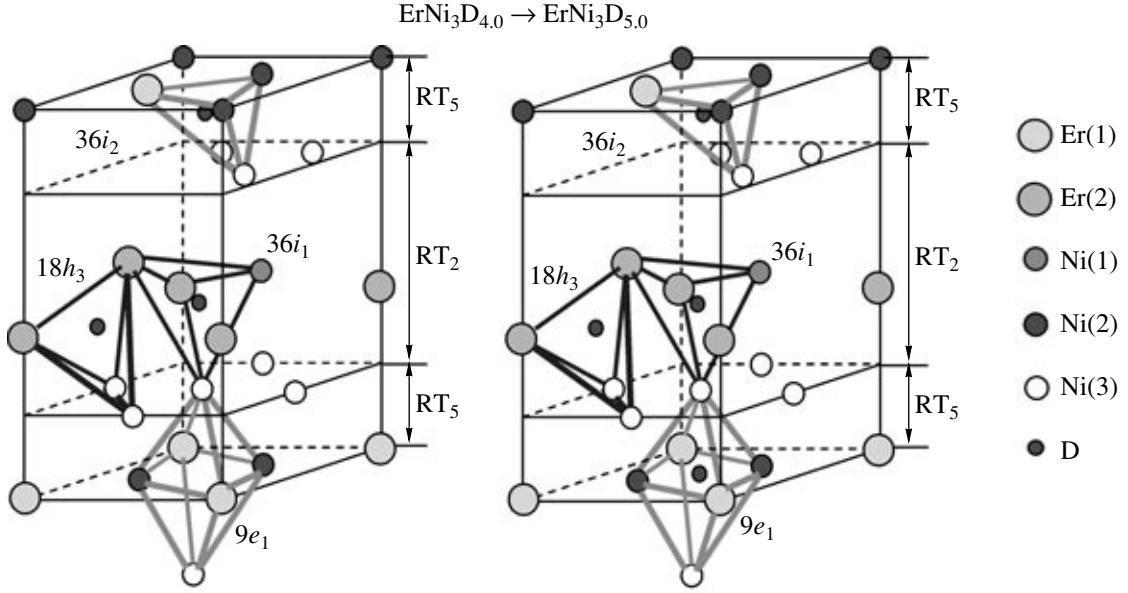

Fig. 5. Hydrogen sites in hydrided $ErNi_3$.

Comparison of hydrogen arrangement in the $MgZn_2$-type blocks of $PuNi_3$-type structures with that in $MgZn_2$-type structures, in which hydrogen resides predominantly in positions k and l [13] (corresponding to positions i and h_3 in $PuNi_3$ [5]), indicates that, in the structures of $ErNi_3$ and $CeCo_3$, the k sites adjacent to l sites have low occupancies. Previous work [14] has shown that, in the hexagonal Laves phase structure C14, the hydrogen occupancy on the k and l sites depends on the blocking radius R_L and interatomic distances: the k sites are partially occupied at small $R_L$and empty at large R_L. It seems likely that the zero occupancy of the k sites adjacent to l sites in all of the compounds with the $PuNi_3$ structure [1–5] is due to blocking.

In the high-pressure hydrides $ErNi_3D_{5.0}$ and $CeCo_3D_{6.0}$, hydrogen occupies new sites (including octahedral ones). In addition, the hydrogen occupancies of the partially occupied sites are higher (Tables 3, 4). The new sites are located in the RT_5 block (Figs. 4, 5),

Table 4. Coordination and types of interstices in hydrides with the $PuNi_3$ structure

Position, occupancy											Coordination of interstices	Structural block
1	2	3	4	5	6	7	8	9	10	11		
–	–	$6c_1$ 0.95	$6c_1$ 0.39	$6c_1$ 0.06	–	–	–	–	$6c_1$ 0.88	$6c_1$ 0.78	RM_3	RT_2
–	–	–	–	$6c_3$ 0.49	$6c_3$ 0.24		–	–	–	–	M_4	RT_2
–	–	–	–	–	–		–	–	$18h_1$ 0.15	$18h_1$ 0.78	R_2M_2	RT_2 and RT_5
–	–	–	$18h_2$ 0.15	$18h_2$ 0.48	$18h_2$ 0.26	$18h_2$ 0.20	$18h_2$ 0.24	$18h_2$ 0.84	–	–	R_2M_2	RT_2 and RT_5
$18h_3$ 0.20	$18h_3$ 0.26	–	–	$18h_3$ 0.19	$18h_3$ 0.11		–	–	–	–	R_2M_2	RT_2
–	–	–	–	–	$18h_6$ 0.07		–	–	$18h_6$ 0.22	–	R_2M_2	RT_2
$36i_1$ 0.70	$36i_1$ 0.80	$36i_1$ 0.92	$36i_1$ 0.57	$36i_1$ 0.38	$36i_1$ 0.24	$36i_1$ 0.40	$36i_1$ 0.69	$36i_1$ 0.70	$36i_1$ 0.27	–	R_2M_2	RT_2
–	–	–	–	–	$6c_4$ 0.33		–	–	–	–	M_4	RT_5
–	–	–	$18h_5$ 0.14	$18h_5$ 0.36	$18h_5$ 0.52		–	–	–	–	RM_3	RT_5
$36i_2$ 0.10	$36i_2$ 0.12	–	–	–	$36i_2$ 0.22	$36i_2$ 0.28	–	$36i_2$ 0.08	–	–	RM_3	RT_5
–	$9e_1$ 0.70	–	–	–	–	$9e_1$ 0.11	–	–	–	–	R_2M_4	RT_5

Note: (1) $ErNi_3D_{4.0}$, (2) $ErNi_3D_{5.0}$, (3) $ErNi_3D_{1.23}$ [2], (4) $ErNi_3D_{1.97}$ [2], (5) $ErNi_3D_{3.75}$ [2], (6) $LaY_2Ni_9D_{12.8}$ [5], (7) $CeCo_3D_{6.0}$, (8) $CeCo_3D_{4.0}$, (9) $ErCo_3D_{4.0}$ [4], (10) $CeY_2Ni_9D_{7.7}$ [5], (11) $HoNi_3D_{1.8}$ [1].

while the sites of the first type (in the RT_2 block and between the blocks) remain partially occupied. The incorporation of hydrogen into interstices of the RT_5 block at high pressures leads to its expansion by about 10% (Table 1), while the RT_2 block contracts slightly along the *c* axis, and the *a* parameter increases in both high-pressure hydrides. All sites of the same type cannot be occupied because of the interaction between hydrogen atoms in neighboring sites, which is significant at high hydrogen contents, i.e., in $ErNi_3D_{5.0}$ and $CeCo_3D_{6.0}$. Comparison of the interstice radii in the structures of the intermetallic compounds and low- and high-pressure hydrides indicates that, in the low-pressure hydrides, the radius of partially filled sites in the RT_5 block increases, favoring hydrogen incorporation into new sites in hydrogen-rich hydrides.

Using x-ray spectroscopy, Stange et al. [15] analyzed the valence state of Ce in Ce-containing intermetallics and hydrides with the aim of assessing the effect of changes in Ce valence on the hydrogen-induced volume effect. The hydriding of Ce-containing intermetallics changes the electronic configuration of Ce, $4f^0 \longrightarrow 4f^1$, and, accordingly, its ionic radius, from $r = 0.1715$ nm (Ce^{4+}) to $r = 0.1825$ nm (Ce^{3+}), thereby contributing to the lattice expansion of the hydride. The Ce valence in hydrides was found to be essentially constant, at 3.12–3.18 in hydrides with the $CeNi_3$ structure and 3.32 in hydrides with the $PuNi_3$ structure. This suggests that the large changes in unit-cell volume (about 30%) in Ce-containing hydrides are essentially unrelated to the valence state of Ce.

Thus, neither the nature of the sites occupied by hydrogen nor the sequence in which they are filled accounts for the difference in anisotropy and volume effect between the hydrides under consideration. Analysis of interatomic distances sheds some light on this problem. For all of the hydrogen sites in $ErNi_3D_{4.0}$ and most of the hydrogen sites in $CeCo_3D_{4.0}$, all of the variations from hydrides of the constituent metals reduce to a more or less uniform increase in R–H and T–H bond lengths, with the hydrogen atoms residing essentially in the center position of the interstices. In all cases, the "heredity" principle, proposed in [9, 16, 17], is met: the interatomic distances in intermetallic hydrides are close to those in binary hydrides (Table 5, Fig. 6a).

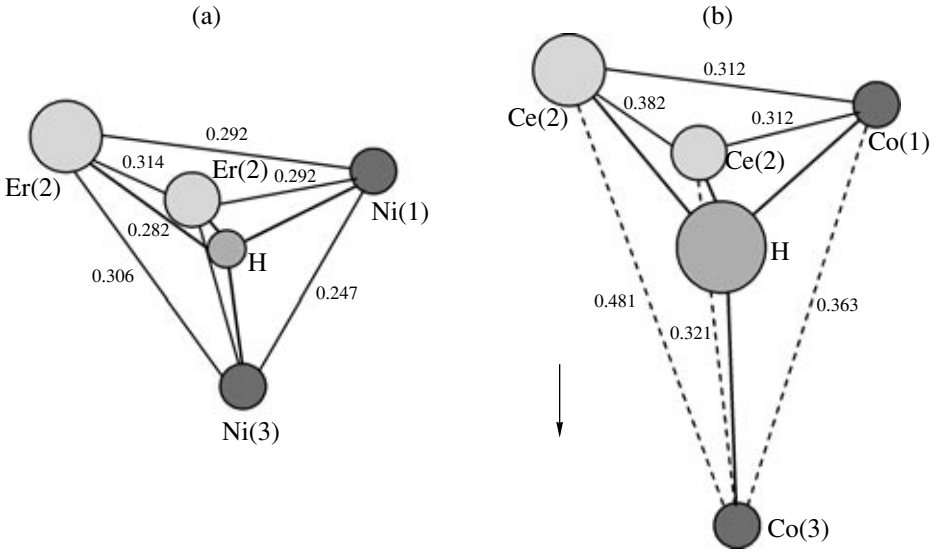

Fig. 6. Hydrogen atom in position $36i_1$ in (a) $ErNi_3H_{4.0}$ (small lattice anisotropy) and (b) $CeCo_3H_{4.0}$ (large anisotropy).

A completely different situation occurs in the case of position $36i_1$ in the RT_2 block, which has the highest occupancy in hydrided $CeCo_3$. The R–H bond lengths here (Fig. 6b) are nearly the same (or slightly larger) as in the corresponding binary hydride, while one of the Co–H bonds is markedly longer in comparison with the binary hydride and, accordingly, the R–T bonds are weaker (Fig. 6b, dashed lines), which is accompanied by large anisotropy (large *c*/*a* ratio). The hydrogens in this intermetallic hydride are shifted from the center position of their tetrahedra toward the cerium-containing plane. This implies that the hydrogen in this position is in the state $H^{z+\delta}$ ($r < 0.2$ nm), which leads to an increase in T bond length. In other words, the hydrogen acts as a "trigger," which scavenges electrons from rare-earth ions and conveys them to T ions, that is, empties the *sp* band and dopes the *d* band of the hydride (Fig. 7). Clearly, this effect must be stronger in com-

Table 5. Bond lengths in RT_3 compounds and their deuterides (hydrogen atoms in position $36i_1$)

d, nm				
$CeCo_3$	$CeCo_3D_{4.0}$		$CeCo_3D_{6.0}$	
Ce(2)–Ce(2) 0.255	Ce(2)–Ce(2) 0.382	Ce(2)–D 0.255	Ce(2)–Ce(2) 0.387	Ce(2)–D 0.268
Ce(2)–Co(3) 0.251	Ce(2)–Co(3) 0.481	Ce(2)–D 0.251	Ce(2)–Co(3) 0.323	Ce(2)–D 0.230
Ce(2)–Co(3) 0.251	Ce(2)–Co(3) 0.321	Co(3)–D 0.253	Ce(2)–Co(3) 0.485	Co(3)–D 0.213
Ce(2)–Co(1) 0.251	Ce(2)–Co(1) 0.312	Co(1)–D 0.166	Ce(2)–Co(1) 0.315	Co(1)–D 0.189
Co(3)–Co(1) 0.253	Co(3)–Co(1) 0.363		Co(3)–Co(1) 0.366	
$ErNi_3$	$ErNi_3D_{4.0}$		$ErNi_3D_{5.0}$	
Er(2)–Er(2) 0.299	Er(2)–Er(2) 0.314	Er(2)–D 0.243	Er(2)–Er(2) 0.342	Er(2)–D 0.245
Er(2)–Ni(3) 0.295	Er(2)–Ni(3) 0.306	Er(2)–D 0.225	Er(2)–Ni(3) 0.310	Er(2)–D 0.220
Er(2)–Ni(3) 0.295	Er(2)–Ni(3) 0.282	Ni(3)–D 0.148	Er(2)–Ni(3) 0.289	Ni(3)–D 0.153
Er(2)–Ni(1) 0.289	Er(2)–Ni(1) 0.292	Ni(1)–D 0.152	Er(2)–Ni(1) 0.315	Ni(1)–D 0.159
Ni(3)–Ni(1) 0.232	Ni(3)–Ni(1) 0.247		Ni(3)–Ni(1) 2.77	

Notes: Bond lengths (nm) in $ErFe_2D_5$ [19]: Er–Er 0.345, Fe–Fe 0.278, Er–Fe 0.333, Er–D 0.183, Fe–D 0.186; in $LaCo_5D_6$ [20]: La–La 0.409, Co–Co 0.235, La–Co 0.293, La–D 0.262, Co–D 0.173; in $LaNi_5D_6$ [21]: La–La 0.420, Ni–Ni 0.265, La–Ni 0.312, La–D 0.256, Ni–D 0.165.

M–H bond lengths (nm) in binary hydrides [16]: 0.222 in ErH_2, 0.242 in CeH_2, 0.182 in NiH, 0.186 in CoH.

Fig. 7. Changes in atomic radii in going from (a) $ErNi_3H_{4.0}$ (small lattice anisotropy) to (b) $CeCo_3H_{4.0}$ (large anisotropy).

pounds containing light rare-earth ions (La, Ce, Pr, Nd), which readily give up electrons to the *sp* band and have a tendency to form R^{4+} valence states (Ce, Pr), and must be weaker in compounds of heavy rare-earth metals (Dy, Ho, Er), which are more likely to be in the valence state 2+. Moreover, this effect must be stronger for T ions with a higher density of states in the *d* band. Finally, it must be stronger for sites with R_2T_2 coordination with a high rare-earth content of the RT_2 block and must be weaker for sites with RT_3 coordination in the RT_5 block with a lower rare-earth content, which accounts for the difference in anisotropy between compounds in which one or both structural blocks are occupied [1–5].

It follows from this approach and structural data that the hydrogen in $PuNi_3$-structure hydrides is in two different charge states: formally "anionic," with $r \simeq 0.2$ nm and $z \simeq -1$, in the RT_2 structural component, and formally "metallic," with $r \simeq 0.056$ nm and $z \simeq 0^{\delta+}$, in the RT_5 structural component. This behavior reflects the difference in the nature of the interaction between hydrogen and the constituent metals of intermetallics: hydrogen acts as an electron acceptor for rare-earth metals and as a donor for transition metals. In addition, this behavior accounts, qualitatively and may be quantitatively, for the observed volume effect and anisotropy in intermetallic hydrides with block structures. The notion that the hydrogen–metal bonds in intermetallic hydrides are heteropolar and that their nature depends on hydrogen content was formulated by Semenenko and Burnasheva [18] long ago, based on tentative data on the hydrogen distribution in the lattice. Later work [9, 16, 17], directed toward analysis of the hydrogen-induced volume effect in rare-earth and transition-metal hydrides, as well as in intermetallic hydrides containing rare earths and transition metals, revealed different behaviors of light and heavy rare-earth ions and culminated in the "heredity" principle for interatomic distances in intermetallic hydrides. The present results support, develop, and refine earlier observations.

CONCLUSIONS

Structural characterization of the intermetallic compounds $CeCo_3$ and $ErNi_3$ hydrided at different hydrogen pressures and analysis of earlier data for similar, isostructural systems indicate that hydrogenation leads to the formation of hydrides based on the parent compounds with the $PuNi_3$ structure. The hydrogen in these hydrides first occupies R_2T_2-coordinated interstitial sites in the $MgZn_2$-type structural blocks, then, R_2T_2 sites between the $MgZn_2$ and $CaCu_5$ blocks, and, finally, RT_3 sites in the $CaCu_5$ blocks. The sites adjacent to the occupied sites are then empty or occupied only partially.

Hydrogenation is accompanied by an increase in the unit-cell volume and anisotropic expansion of the lattice of the parent intermetallic compound, which is strong for intermetallics containing light rare-earth metals and weak for those containing heavy rare-earth metals. Our results demonstrate that this behavior is associated with the difference in the nature of hydrogen–metal bonds, which are predominantly ionic for rare-earth metals (hydrogen acts as an acceptor) and predominantly metallic for transition metals (hydrogen acts as a donor), and must be accompanied by emptying of the *sp* band and filling of the *d* band.

ACKNOWLEDGMENTS

This work was supported by the Russian Foundation for Basic Research, grant nos. 03-03-33023 and 03-02-17387.

REFERENCES

1. Burnasheva, V.V., Yartys', V.A., Solov'ev, S.P., et al., Neutron Diffraction Study of the Crystal Structure of $HoNi_3D_{1.8}$, *Kristallografiya*, 1982, vol. 27, no. 4, pp. 680–685.
2. Filinchuk, Y.E. and Yvon, K., Directional Metal–Hydrogen Bonding in Interstitial Hydrides, I-$ErNi_3H_x$ ($0 < x < 3.7$), *J. Alloys Compd.,* 2005, vols. 404–406, pp. 89–94.
3. Van Essen, R.H. and Buschow, K.H.J., Hydrogen Sorption Characteristics of Ce–3*d* and Y–3*d* Intermetallic Compounds, *J. Less-Common Met.*, 1980, vol. 70, pp. 189–198.
4. Bartashevich, M.I., Pirogov, A.N., and Voronin, V.I., Crystal Structure of γ-Phase $RCo_3H_{\sim 4}$ Hydrides, *J. Alloys Compd.*, 1995, vol. 231, pp. 104–107.
5. Latroche, M., Paul-Boncour, V., and Percheron-Guegan, A., Structural Properties of Two Deuterides $LaY_2Ni_9D_{12.8}$ and $CeY_2Ni_9D_{7.7}$ Determined by Neutron Powder Diffraction and X-ray Spectroscopy, *J. Solid State Chem.*, 2004, vol. 177, pp. 2542–2549.

6. Klyamkin, S.N. and Verbetsky, V.N., Interaction of Intermetallic Compounds with Hydrogen up to 250 MPa: $LaCo_{5-x}Mn_x$–H_2 and $CeNi_5$–H_2 Systems, *J. Alloys Compd.*, 1993, vol. 194, pp. 41–45.
7. Taylor, K.N.R., Intermetallic Rare-Earth Compounds, *Adv. Phys.*, 1971, vol. 20, no. 87, pp. 551–660.
8. Verbetsky, V.N., Klyamkin, S.N., Kovriga, A.Yu., and Bespalov, A.P., Hydrogen Interaction with RNi_3 Type Intermetallic Compounds at High Gaseous Pressure, *Int. J. Hydrogen Energy*, 1996, vols. 11–12, pp. 997–1000.
9. Somenkov, V.A and Shilshtein, S.Sh., Hydrogen-Induced Volume Changes in Transition Metals and Intermetallic Compounds, *Fiz. Met. Metalloved.*, 1998, vol. 86, no. 3, pp. 114–122.
10. Burnasheva, V.V., Tarasov, B.P., and Semenenko, K.N., RNi_3–H_2 (R = Light Rare Earth) Hydrides, *Zh. Neorg. Khim.*, 1982, vol. 27, no. 12, pp. 3039–3042.
11. Shilov, A.L., Yaropolova, E.I., and Kost, M.E., Hydrides Based on SmM_3 (M = Co, Ni, Ru) Compounds, *Dokl. Akad. Nauk SSSR*, 1980, vol. 252, no. 6, pp. 1397–1400.
12. Burnasheva, V.V. and Tarasov, B.P., Hydrogen Absorption in RNi_3 (R = Heavy Lanthanide) Intermetallic Compounds, *Zh. Neorg. Khim.*, 1982, vol. 27, no. 8, pp. 1906–1910.
13. Souberoux, J.L., Fruchart, D., and Biris, A.S., Structural Studies of Laves Phases $ZrVCo(V_{1-x}Cr_x)$ with $0 < x < 1$ and Their Hydrides, *J. Alloys Compd.*, 1999, vols. 293–295, pp. 88–92.
14. Lushnikov, S.A., Verbetsky, V.N., Glaskov, V.P., and Somenkov, V.A., Structure of $NbVCoD_{2.5}$ Synthesized under High Gaseous Pressure, *IX Int. Conf. Hydrogen Materials Science and Chemistry of Carbon Nanomaterials*, Sevastopol, 2005.
15. Stange, M., Paul-Bouncour, V., Latroche, M., et al., Ce-Valence State and Hydrogen-Induced Volume Effects in Ce-Based Intermetallic Compounds and Their Hydrides, *J. Alloys Compd.*, 2005, vols. 404–406, pp. 144–149.
16. Somenkov, V.A. and Irodova, A.V., Lattice Structure and Phase Transitions of Hydrogen Compounds, *J. Less-Common Met.*, 1984, vol. 101, pp. 481–484.
17. Somenkov, V.A. and Shilshtein, S.Sh., Structural Aspects of Behavior of Hydrogen in Metals and Intermetallic Compounds, *Phys. Chem.*, 1979, vol. 117, pp. 125–129.
18. Semenenko, K.N. and Burnasheva, V.V., Synthesis and Phase Transformations of Metal Hydrides, *Vestn. Mosk. Univ., Ser. 2: Khim.*, 1977, vol. 18, no. 5, pp. 618–632.
19. Paul-Bouncour, V., Filipek, S.M., Percheron-Guegan, A., et al., Structural and Magnetic Properties of RFe_2H_5 Hydrides, *J. Alloys Compd.*, 2001, vols. 317–318, pp. 83–87.
20. Kuijpers, F.A. and Loopsta, B.O., A Neutron-Diffraction Study on the Structural Relationships of RCo_5 Hydrides, *J. Phys. Chem. Solids*, 1974, vol. 35, pp. 301–306.
21. Yartys, V.A., Burnasheva, V.V., Semenenko, K.N., et al., Crystal Chemistry of $RT_5H(D)_x$, $RT_2H(D)_x$, and $RT_3H(D)_x$ Hydrides, Based on Intermetallic Compounds of $CaCu_5$, $MgCu_2$, $MgZn_2$, and $PuNi_3$ Structure Types, *Int. J. Hydrogen Energy*, 1982, vol. 7, no. 12, pp. 957–965.